Construction and Building Materials 338 (2022) 127349

Contents lists available at ScienceDirect

Construction and Building Materials

journal homepage: www.elsevier.com/locate/conbuildmat

Photocatalytic TiO_2 nanosheets-SiO_2 coatings on concrete and limestone: An enhancement of de-polluting and self-cleaning properties by nanoparticle design

M. Luna [a,1], J.J. Delgado [b,1,*], I. Romero [b,c], T. Montini [c], M.L. Almoraima Gil [a], J. Martínez-López [d], P. Fornasiero [c], M.J. Mosquera [a,*]

[a] Departamento de Química Física, Facultad de Ciencias, Universidad de Cadiz, Campus Río San Pedro, Puerto Real (Cádiz), E-11510, Spain
[b] Departamento de Ciencia de los Materiales, Ingeniería Metalúrgica y Química, Inorgánica, Facultad de Ciencias del Mar y Ambientales, Universidad de Cadiz, Campus Río San Pedro, Puerto Real (Cádiz), E-11510, Spain
[c] Department of Chemical and Pharmaceutical Sciences, ICCOM-CNR, Consortium INSTM, University of Trieste, 34127 Trieste, Italy
[d] Departamento de Ciencias de la Tierra, Facultad de Ciencias, Universidad de Cadiz, Campus Río San Pedro, Puerto Real (Cádiz), E-11510, Spain

ARTICLE INFO

Keywords:
TiO_2 nanosheets
Self-cleaning nanomaterials
Photocatalysis
photocatalytic NO_x abatement
Photo-catalytic soot removal

ABSTRACT

In this study, we develop TiO_2-SiO_2 nanocomposites that can be employed as photoactive coatings to create surfaces with antipollution and self-cleaning properties in urban buildings. In particular, anatase titanium dioxide with a high percentage of {001} facets, commonly called titania nanosheet (TNS), was used as active phase. This approach allows us to improve the antipollution properties of similar sols based on P25. The obtained TNS were intensively characterized by UV–Vis diffuse reflectance absorption, X-Ray diffraction and transmission electron microscopy to rationalize the sol synthesis and fully understand the photocatalytic performances. Our results clearly show that after treating the titania nanosheets with NaOH to remove adsorbed residual fluoride from the synthesis, they can be easily dispersed and the photocatalytic activity is dramatically improved. This material has been shown to effectively reduce concentrations of NO_x, soot and organic dyes under simulated sun light radiation.

1. Introduction

During the last decades, there has been a growing interest in proposing eco-sustainable strategies to mitigate the human impact on the environment. Special attention has been paid to solve the air pollution problems in populated urban areas. In this sense, around 7000 kilotons of nitrogen oxides (NO_x = NO + NO_2) and 200 kilotons of soot are emitted annually in Europe [1]. These pollutants have a direct impact on the people health promoting the development of cancer and respiratory diseases [2]. In 2018, 55,000 and 417,000 premature deaths in Europe were attributed to NO_2 (more toxic than NO) and $P.M_{25}$ (particulate matter smaller than 2.5 μm, whose one of their components is soot), respectively [3]. For this reason, the governments are adopting actions in order to improve the air quality in big cities, for instance the establishment of low emission zones [4].

In this context, the photocatalysis opens a wide range of possibilities allowing to harness the solar energy in order to induce sustainable redox transformations [5]. Among all photocatalysts, special attention has been paid to TiO_2 due to its properties, such as lack of toxicity, high physicochemical stability, low cost, high availability and good photocatalytic activity [6]. TiO_2 has also been proposed as smart component in building materials to obtain attractive properties such as the self-cleaning, biocide and de-polluting effects [7]. Remarkably, TiO_2 has relevant capacity of degrading a wide range of pollutants and the TiO_2-based photocatalytic materials are currently investigated and tested to improve the quality of the air of polluted cities [8,9]. However, TiO_2 effectiveness in outdoors applications is limited due to its light absorption restricted to the UV range, which is relatively scarce in the sunlight. For this reason, an important field of the current research is focussed on enhancing visible light absorption. Common strategies includes metal deposition, doping with metals or non-metals or dye sensitization [10]. Many of these modifications lead to the desired improvement in visible

* Corresponding authors.
E-mail addresses: juanjose.delgado@uca.es (J.J. Delgado), mariajesus.mosquera@uca.es (M.J. Mosquera).
[1] Both authors contributed equally to this work.

https://doi.org/10.1016/j.conbuildmat.2022.127349
Received 15 December 2021; Received in revised form 21 March 2022; Accepted 29 March 2022
Available online 28 April 2022

light absorption that can be easily visualized by a colour change from white to yellowish or even blueish. While these colour variations are perfectly compatible with some photocatalytic applications, the application of coloured TiO_2 in building materials is less simple especially in historical buildings or construction based on natural stones, where typically thin layers of white titania are used as they act as a nearly transparent protective and self-cleaning shield that also actively reduce the air pollution [11]. The colour alteration of building materials is typically quantified by measuring the total colour difference (ΔE^*) parameter from the chromaticity coordinates of the CIE 1976 L*a*b* colour space [12]. This is a relevant factor for certain applications where the original appearance of the substrate must be preserved, such as the application on heritage building or monuments. In these situations, the total colour difference value lower than 3 is desirable and 5 is frequently the tolerable upper limit [13]. Therefore, improving the photocatalyst efficiency without shifting the band gap to the visible region is of paramount importance. In this respect, the photocatalytic activity of TiO_2 is also strongly affected by its structure, thus other strategies for enhancing its performances can and must be considered, such as the optimization of the synthetic procedures to obtain well-defined nanostructured material. Specifically, amorphous TiO_2 doesn't exhibit photoactivity, while crystalline phases, such as rutile, anatase and brookite, presents are active photocatalysts [14]. Anatase is more active than rutile due to its higher surface area and indirect-type band gap that increase the lifetime of electron-hole pairs. On the other hand, brookite has emerged as an even more promising photocatalyst than anatase and rutile, but the number of studies about this phase is much lower than that on the other polymorphs. The TiO_2 particle size and shape [15,16] strongly affects the photoactivity being the control of morphology a key factor in the TiO_2 photocatalysts preparation. These two aspects are related with TiO_2 surface: (1) the small size provides great surface-to-volume ratios that increases the number of active centres and (2) the shapes are related with the exposure of specific facets. This last aspect is particularly important because large faceted particles can show higher activity than much smaller spherical particles, due to the particular properties of each facet [17].

{0 0 1}, {0 1 0} and {1 0 1} are the main low-index facets that we can find in anatase crystals [17]. Specifically, the {0 0 1} facets are the most reactive because this surface attracts holes and has atoms with low coordination, favouring the photocatalytic oxidation activity. However, this is the less stable surface with a surface energy which is almost doubled that those of the corresponding {0 1 0} and {1 0 1} surfaces. Therefore, a regular crystal growth produces particles primarily dominated by the less reactive and more thermodynamically stable {1 0 1} and {0 1 0} facets. The obtainment of anatase crystals with a high percentage of {0 0 1} facets requires synthetic procedures that employ capping agents able to stabilize this surface promoting its growth [17]. {0 0 1}-faceted TiO_2 nanosheets has been previously stated as an excellent photocatalyst for the degradation of organic compound. In fact, its photocatalytic activities are considerably higher than the exhibited by the commercial P25. Despite these promising results, there are no clear advances in the use of these nanomaterials in real applications.

The integration of TiO_2 in building materials requires additional attention, starting from considering the differences between their inclusion in existing building from that of their used in new constructions. In both cases, the photoactive component must be incorporated on the surface and not in the bulk of concrete as its activity is expressed only interacting with light and adsorbed species [18–20]. Therefore, the easiest way to effectively use TiO_2 in constructions is to make a fine dispersion of TiO_2 nanomaterials in a solvent to be used for creating photoactive coatings after the evaporation of the solvent. Typically, these types of coatings exhibit a progressive decrease in performances as the TiO_2 nanoparticles can be easily detached due to the weather effects [21,22]. This problem can be mitigated by using silica as binder, which has a high affinity for TiO_2 and most of the common building materials [23]. Moreover, SiO_2 normally exhibited high surface area and porous structure that allows the diffusion of the pollutants to the photoactive centres, improving the performance in comparison with a non-porous matrix [23].

In view of the above considerations, we propose in this work the integration of {0 0 1}-faceted TiO_2 nanosheets in a silica sol for producing TiO_2-SiO_2 photocatalytic coatings for building materials with enhanced photoactivity with respect to that of commercial P25 TiO_2 benchmark. Specifically, we show that it is possible to easily obtain morphologically controlled TiO_2 nanoparticles by solvothermal synthesis and that it can be effectively integrated in a SiO_2 sol during a sol–gel process. Finally, a homogeneous xerogel was obtained by incorporating the TiO_2 nanosheets. The use of sol-gels has been already proven as an effective methodology for treating in-situ the building materials. This is mainly due to the fact that the sol can easily penetrate into the porous structure of the stone producing spontaneously xerogels coatings with high adhesion. Additionally, and taking advantage of their low viscosity, they can be applied in situ by common methods such as spraying. The application of this material as an active building element for the air purification (soot and NO_x removal) with self-cleaning (decomposition of soot and dye stains) properties is discussed and our results show that titania nanosheets can be used in real applications.

2. Experimental

2.1. Catalyst preparation

2.1.1. Synthesis of titania nanosheets.

TiO_2 anatase single crystal nanosheets were synthesized by adapting the procedure reported by Yang et al [24]. First, 60 mL of 2-propanol (2-PrOH) and 18 mL of tetrabutyl titanate $Ti(C_4H_9O)_4$ were mixed into a 150 mL Teflon-lined autoclave. Finally, 2.16 mL of HF (48 wt%) as a capping agent were added dropwise under stirring using a micropipette. The nominal molar ratio of HF to $Ti(C_4H_9O)_4$ was kept constant (2:1). After mixing the solution for 30 min, the Teflon-lined autoclave was placed in the oven for a solvothermal treatment at 180 °C for 24 h. After that, the products were carefully collected and washed three times with a mixture of H_2O MilliQ and ethanol (EtOH) (50:50) in a centrifuge at 4500 rpm and then dried overnight in an oven at 70 °C.

In order to investigate the effect of surface fluorination on photoactivity, the TiO_2 nanosheets were treated with diluted (0.01 M) NaOH solution to remove fluoride ions form the surface. The TiO_2 powder (0.5 g) was placed in a plastic beaker, NaOH solution was added (50 mL) and magnetically stirred in the dark for 12 h. Then, the samples were filtered and washed with a dilute HCl solution (25 mL; twice) to eliminate Na^+ ions and with subsequently with MilliQ water until no Cl^- ions were detected in the mother liquor (test with $AgNO_3$). The treatment has been repeated 4 times, in order to ensure significant removal of fluoride ions. Finally, the samples were dried at 60 °C overnight. The F^- ions samples were removed from the surface of TiO_2 via the reaction (1):

$$\text{Bulk-Ti} - \text{F} + \text{OH}^- \rightarrow \text{Bulk-Ti} - \text{OH} + \text{F}^- \quad (1).$$

The as synthetized sample will be denoted as NS, while the sample prepared by removing surface fluoride by the NaOH treatment will be labelled as NSNaOH.

2.1.2. Synthesis of the self-cleaning titania based products.

The prepared TiO_2 was mixed with a silica precursor, TES40 WN (Wacker), an ethylsilicate oligomer that provides approximately 41% of silica upon complete hydrolysis, following a previously established procedure [25]. The amount of TiO_2 particles added to the synthesis were 1 and 4 g per 100 mL of TES40. For comparative purposes, an only silica sol without titania and sols using the commercial P25 particles from Evonik were prepared. The sols were designated S&XXX, where & refers to the TiO_2 mass/volume % in the sol and XXX is an identifying tag of the type of TiO_2 particles employed. 15 mL of the synthetized sols were disposed in plastic Petri dishes where the sol–gel transition took place at laboratory conditions. Finally, the gels were dried at the same

conditions until not weight lost was observed.

For the treatment evaluation, a stone called Capri limestone was chosen. This building material quarried from Spain is composed by calcite and it has an open porosity of 9–12%. It presents a very clear beige-white colour and it is frequently employed in exterior paving and façade facing. The sols were applied on 5x5x2 cm pieces of the substrate by spraying onto one of the larger faces until the substrate stops absorbing the product and the sol starts to be accumulated on the sample surface. The surface was maintained wet for 1 min and the sol excess was removed using compressed air. The treated stones were dried at 18 ± 0.5 °C and 53 ± 3% of relative humidity until constant weight (approximately after two weeks).

The NO depolluting properties of the treatments were evaluated using concrete, the specimens were prepared using CEM II/B-L 32.5 N portland cement, siliceous sand (0.1–2 mm) and limestone aggregates (6–12 mm) purchased in a local building material warehouse. The mass mix proportions used for preparing the concrete samples were 1:2:2:0.6 (cement:sand:aggregates:water). The mixture was cast on 120 mm plastic petri dishes, the concrete plates was unmoulded after 24 h, they were cured under ambient conditions for 28 days and they were cut into 10x5x1.4 cm pieces. Finally, 40 mg·cm^{-2} of the product was deposited on the surface of the concrete and dried over night at 60 °C.

2.2. Physical and chemical characterization

XRD patterns of TiO_2 nanosheets were collected using a Bruker diffractometer AXS, model D8 Advance, equipped with a Cu-$K_{\alpha 1}$ radiation source operated at 50 kV and 50 mA. The diffractograms were registered from 3° to 78° during 1 h. The Rietveld analysis was performed using the software TOPAS 5.0 (Bruker AXS). Photo-catalysts were also analyzed by transmission electron microscopy (TEM) using a TEM/STEM FEI Talos F200X G2 microscope (Thermo Fisher Scientific, Waltham, MA, USA). HAADF-STEM images and XEDS maps were obtained thanks to a 4 Super-X SDDs. Elemental maps were acquired with a beam current of approximately 90 pA and a dwell time of 75 µs. A FEI Nova 450 electron microscope with an accelerating voltage of 3 kV was used to record the Scanning Electron Microscopy (SEM) images.

Brunauer-Emmet-Teller (BET) specific surface areas of the catalysts were measured by nitrogen physisorption at liquid nitrogen temperature on an Autosorb®iQ instrument from Quantachrome. Approximately 0.3 g of sample, previously evacuated at 150 °C overnight, were employed in the analysis. The corresponding pore size distributions were calculated using a hybrid NLDFT (non-local density functional theory) approach [26] considering the absorption of N_2 on silica with cylindrical pores. The UV–Vis diffuse reflectance spectra of the samples were obtained using a doubled beam Varian Carry 5000 spectrophotometer using an integrating sphere.

A viscometer (model DV-II + with UL/Y adapter) from Brookfield operated at 25 °C was employed for evaluating the rheological properties of the sols immediately after the synthesis. The viscosities values were determined as the slope of shear stress vs. shear rate curves in their ranges of Newtonian behaviour evaluated.

The colour changes in the substrates induced by the treatments with the obtained self-cleaning products were determined by using a solid reflection spectrophotometer, Colorflex model, from HunterLab. The conditions were illuminant D65 and observer 10°. The colour changes were quantifying using the CIELa*b* colour space and the total colour difference (ΔE*) parameter.

2.3. Evaluation of the photo-catalytic self-cleaning properties and abatement of NO_x pollutants.

The photoactivity of the samples were evaluated using a dye photodegradation test. In a typical experiment, 500 µL of a 1 mM solution of methylene blue (MB) in ethanol was deposited dropwise on the treated faces of the limestone samples and it was dried overnight in the darkness at room temperature (around 23 °C). The samples were irradiated in a solar degradation chamber using a power of 500 W/m^2 and the ambient conditions were fixed at 50 ºC and 30 % of relative humidity. The evolution of diffuse reflection spectra of the samples was recorded during the irradiation and the Kubelka-Munk function was employed to determine the MB bleaching. More details about this methodology can be found in a previous work [27].

Soot photo-elimination tests were carried out in order to evaluate the self-cleaning activity of the treated limestone samples. A soot water dispersion (80 mg/L) was prepared using carbon black Printex-U from Evonik, 50 µL/cm^2 and it was deposited on the surface of the studied stones. Subsequently, the samples were dried overnight in an oven at 60 °C. Afterwards, the samples were irradiated with 2 mW/cm^2 of UV irradiation from fluorescent backlight bulb lamps. The evolution of soot stain was monitored during the irradiation digitalizing the stained sample surfaces using an image scanner. The colour of the obtained images was averaged to obtain the corresponding colour coordinates that were employed to calculate the total colour difference of the stained samples using the clean surfaces as reference and the soot degradation was quantified using percentage of colour variation (%$\Delta E^* = 100x\ \Delta E^*/\Delta E^*_0$).

NO photo-oxidation properties were evaluated according to the ISO 22197–1 standard [28]. The reaction mixture was obtained by mixing air and pure NO in the appropriate ratio to get a total flow of 3000 cm^3/min with a NO concentration of 1000 ± 50 ppb. The reaction mixture was introduced into the photocatalytic reactor and, after 45 min, the sample was irradiated using a Osram Ultra Vitalux lamp that provided 10 W/m^2 of UV-A radiation. The NO, NO_x and NO_2 (NO_x-NO) concentrations were determined by chemiluminescence using a model 42i analyser form Thermo Scientific.

3. Results and discussion

3.1. Characterization of titantia nanosheets.

The textural analyses of the bare titania nanosheets were undertaken using nitrogen physisorption technique. The adsorption isotherms of the as-synthetized and washed samples are all very similar. Figure S.1 shows the isotherms of the as-synthetized sample as an example. According to the IUPAC classification [29], it corresponds to Type IV. This type of curve is attributed to mesoporous solids (2 nm < pore size < 50 nm). The hysteresis loop (H1 from the IUPAC classification) is associated with the secondary process of capillary condensation, which results in the complete filling of the mesoporous solid at $P/P_0 < 1$. Type H1 hysteresis is characteristic of solids crossed by channels with uniform sizes and shapes. The obtained BET surface of the as synthetized and NaOH washed samples were 87 and 89 m^2·g^{-1}, respectively. This confirms that the washing treatment doesn't modify the textural properties of the material.

The XRD patterns of the as synthetized and washed samples are identical and both diffractograms can be fitted following the Rietveld analysis assuming a crystal structure of pure anatase (Space Group $I4_1/amd$, n° 141). Fig. 1 includes the experimental result of the as synthetized TiO_2 and the Rietveld refinement, as well as the diffraction pattern of pure anatase phase. The position of the reflections can be reasonably fitted, indicating that the values of the cell parameters obtained by the Rietveld analysis (Table S.1) are reliable and close to the theoretical value. However, some reflections are significantly broader and less intense than expected. This is particularly evident for (1 0 3), (0 0 4), (1 1 2) and (1 0 5) reflections. On the other hand, the (2 0 0) reflection is very sharp and more intense than expected. The unusual width and intensities of some reflections observed in the XRD patterns are in good agreement with the nanosheet morphology. For this reason, the Rietveld refinement procedure used included a model considering the preferential growth along the (2 0 0). Using this approach, a good refinement of the experimental XRD patterns was obtained, although the intensity of

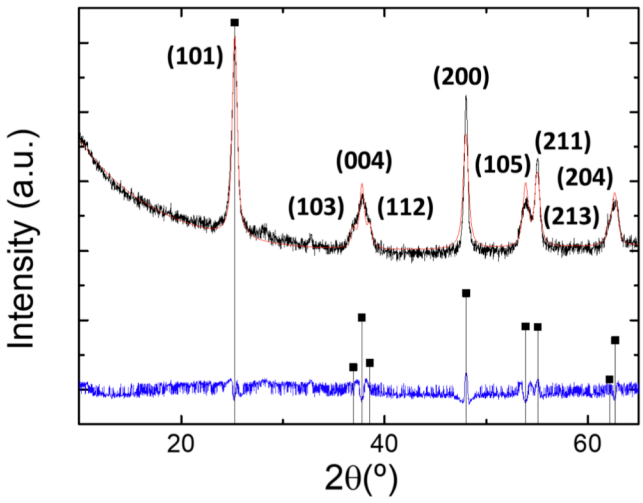

Fig. 1. X-ray diffraction pattern of bare TiO_2 nanosheets (black line), the best fitting results obtained by Rietveld analysis (red line) and the difference between the experimental result and the fitting (blue). Vertical Drop lines correspond to the relative intensities of anatase structure without preferential growth. (For interpretation of the references to color in this figure legend, the reader is referred to the web version of this article.)

the (200) reflection was partially underestimated (Fig. 1). For this reason, the particle size was obtained by analyzing each of the peaks using the LVol-IB method (volume averaged column height calculated from the integral breadth). In order to determinate the nanosheets thickness and length, the crystallite size using the (004) and (200) reflections was obtained and listed in Table S.1.

These data highlights two important features. Firstly, the crystallite size is very large for the reflections with l = 0: (200) and (220). These reflections are originated by families of planes orthogonal to the c axis and parallel to the {001} facets exposed by the nanosheets. In fact, the (200) give us information of the length and the (220) is the diagonal of the nanosheet. Additionally, all the other reflections show smaller crystallite sizes because they correspond to groups of planes that are not orthogonal to the c axis. Notably, crystallite size decreases as the value of l (in hkl) increases. All these features are consistent with the nanosheets morphology having the thinner dimension along the c axis of the anatase structure. In fact, the crystal size obtained for the reflections corresponding to (001) give an estimation of the particles thickness. According to this results, the nanosheets have a length of around 29 nm and a thickness of approximately 8.5 nm.

The morphology and crystal structure of the bare TiO_2 nanosheets were investigated using electron microscopy. Representative SEM images shows the presence of well-defined sheet-shaped TiO_2 particles with a rectangular outline (Fig. 2.A). This result is also confirmed by high resolution HAADF-STEM images. Fig. 2.B shows one nanosheet among the ⟨111⟩ axis zone, while Fig. 2.C can be interpreted by a nanosheet orientated among the ⟨010⟩ axis zone. These results also confirm that the facets of the nanosheet are those labeled in the models included in Figures 2 and S.2. Thanks to this model, an equation to determinate the contribution of the {001} surface to the total surface was obtained (Figure S.2). Additionally, the HAADF-STEM images were used to obtain the particle thickness and length distributions, which are included in Fig. 2.K and 2.L. Regarding, the particle length, we observe values between 15 and 60 nm, being 32 nm the average length of the nanosheets. On the other hand, the thickness distribution was estimated to be centered around 6.5 nm. Applying the previously mentioned equation to obtain the percentage of {001} expose surface and the particle size distribution, we estimated that the contribution of the {001} facets is 75%.

As it was mentioned in the introduction, fluorine may affect the band gap and the photocatalytic activity. For this reason, it was of interest to determinate the fluorine content of the nanosheets by fluorescence (XRF). The as synthetized sample has a fluorine content of 6.1%. The synthesized samples have been treated with diluted NaOH in order to remove fluoride ions from the surface of the materials. This treatment at low temperature was selected instead of thermal treatment at 500 °C to avoid modifications of the morphology and phase composition of the nanosheets. The amount of F^- removed during NaOH treatments was determined by ionic chromatography. The obtained results are presented in Table S.2. These data show that the amount of F^- released during the consecutive NaOH treatments progressively decreased. After the forth treatment, the amount of fluoride detected in the washing solution is negligible, indicating that a further treatment will not further modify the concentration of superficial F in the sample. After the 4 treatments with NaOH solution, the residual F concentration of the sample was 4.1%, that it is still a relatively high content. It's known that F-doped TiO_2 contains different F species, namely surface F ions and bulk/sub-surface F ions [24]. Only the surface F ions can be desorbed by NaOH treatment [30]. In order to confirm that the fluorine remaining after the fourth wash is a bulk species and it is not irreversibly absorbed on the photocatalyst surface, elemental mapping was performing combining HAADF-STEM technique with EDS. Figure S.3 shows the elemental distribution of F and Ti elements in a group of titania nanosheets orientated along the ⟨010⟩ axis zone. We can observe a homogenous distribution of the fluorine in the four times washed sample. In addition, the concentration of fluorine in the inner part of the nanosheet (Area 2) and the total area considering also the surface (Area 1) were 4.2 and 4.6 %, respectively. So, the residual fluorine after NaOH treatment is mostly in the bulk.

The band-gap value was determined using the transformed diffuse reflectance technique according to the Kubelka–Munk theory [31,32]. Figure S.4 presents the UV–Vis absorbance spectra of the as synthetized and washed sample. There is a significant increase in absorption at wavelengths around 350 – 400 nm. The band-gap was obtained assuming an allowed indirect transition. Fig. 3 shows the Tauc's plot for an allowed indirect transition corresponding to both titania nanosheet samples. The obtained band gap value for the as synthetized and washed samples were 3.16 and 3.18 eV, respectively. Those values are very similar and slightly smaller than the value reported in the literature for pure anatase (3.2 eV). Notably, comparable values and a minor effect of F content on band gap have previously been reported for F-doped anatase [33].

3.2. *Characterization of the self-cleaning titania based products.*

The use of different kind of titania in the sol–gel process allowed to appreciate the influence on technological and material processability. In the case of the commercial benchmark P25, homogenous opaque white xerogels were obtained for all the loadings. The use of the as synthetized TiO_2 nanosheets, which contain fluorine on the surface, was more complicate since the nanoparticles are not well dispersed during the synthesis process. The resulting sols were slightly yellow and the nanoparticles of TiO_2 decanted very quickly. In this case, the xerogels were more transparent than those obtained using P25. Optimal situation was achieved with NaOH-washed TiO_2 nanosheets and the P25 nanoparticles for which good and stable dispersion were obtained. Nevertheless, the obtained sols were also translucent and slightly yellow. The difficulties in dispersing the as synthetized nanosheets particles can be related to the high content of surface fluorine, that increase hydrophobic behavior, leading to dispersion problems in both water and organic liquids[34].

The viscosity measured for the sols, as well as their gelation time, are presented in Table 1. All viscosity values are below 7.5 mPa·S and therefore similar to the values that Tegovakon V100 from Evonik, one of the most popular commercial stone consolidants, has (5.25 mPa·s at 25 °C) [35]. These low viscosities are required when the sol application

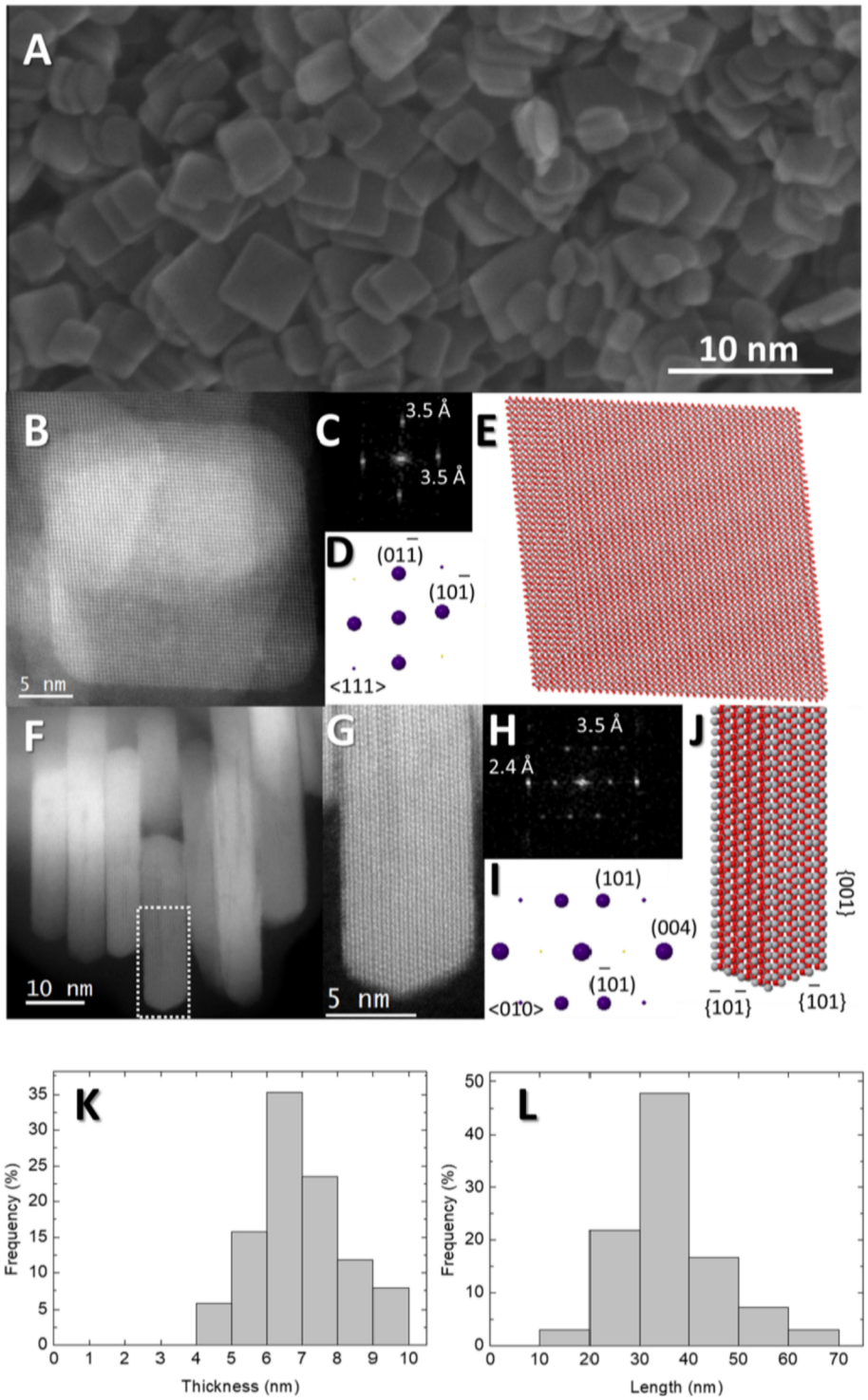

Fig. 2. SEM image obtained by the detection of secondary electrons using a Through-the-lens detector (TLD) (A), high resolution STEM-HAADF of a top (B) and side (F, G) view of the TNS, digital diffraction pattern of the selected area (C, H), simulated electron diffraction pattern (D, I) and atomic model of the nanosheets in the proper orientation (E, J). The thickness (K) and length (L) distribution for bare TiO_2 nanosheets studied in the present work are also included.

will be carried out by common and simple procedures, such as brushing or spraying on buildings and facilitate its penetration in the porous substrate structure increasing the adhesion of the resultant coatings. The lowest viscosity value corresponds to the sample without titania (S) and it increases by adding titania nanoparticles. Although the differences are small between the obtained sols, we can observe two trends; (1) the viscosity was increased as TiO_2 loading was raised and (2) the viscosity was low for the sols containing the as synthetized nanosheets. This last aspect can be easily explained considering that the presence of fluorine leads to flocculation and agglomeration of the titania nanoparticles due to a weak interaction between them and the synthetic solution.

Gelation time may determinate if the material can be used for real applications, because they must be applied in situ and short gelation times creates difficulties to handle the product inhibiting sol penetration into the porous structure of the substrate. In the present case, the lowest gelation time was of 3.5 h, observed using NSNaOH (Table 1). However,

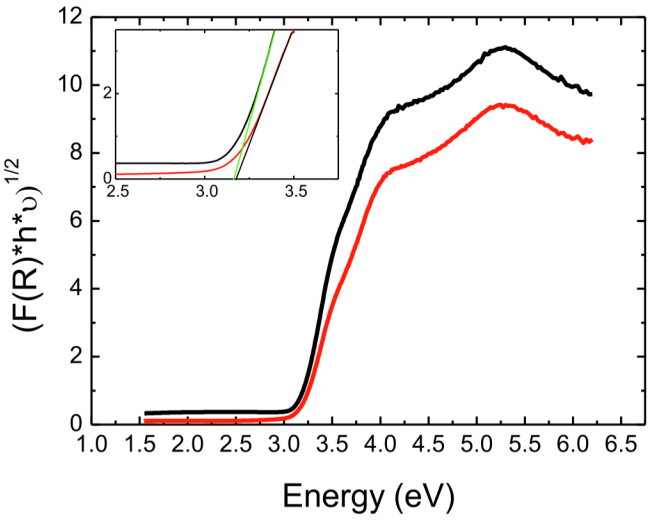

Fig. 3. Taucs plot of the UV–Vis diffuse reflectance absorption spectra of the TNS before (black line) and after washing (red line) assuming an indirect band gap. The inset include the region used for the band gap calculation. (For interpretation of the references to color in this figure legend, the reader is referred to the web version of this article.)

Table 1
Viscosity, gelation time, BET surface area and pore volume (Vp) of all the sol-gels.

Sample	Viscosity (mPa·s)	Gelation Time (h)	Surface (m^2/g)	Vp (cm^3/g)	Pore size (nm)
S	4.62	8	182	0.324	11.3
S1P25	5.51	7	41	0.322	22.5
S4P25	7.17	12	36	0.304	24.5
S1NS	5.06	4.5	103	0.209	8.6
S4NS	5.57	6	116	0.232	8.3
S1NSNaOH	6.02	3.5	154	0.300	8.3
S4NSNaOH	6.28	3.5	156	0.343	8.6

this time is long enough to ensure a good distribution of the sol inside the texture of the stone. Therefore, all the obtained TiO_2-SiO_2 sols are potential candidate for coating building materials. Notably, the addition of only 1% of TiO_2 is enough to strongly reduce the gelation time, as a consequence of the heterogeneous nucleation of silica around TiO_2 species [23,36]. In contrast, for the TiO_2-SiO_2 nanocomposite prepared with 4% TiO_2 P25 and NS, the gelation time increased with respect to the samples with 1%. This could be due to the high affinity of amines for the TiO_2 surface, which reduces the amount of free n-octylamine catalyst in the sol slowing down the sol–gel process [25].

Due to the unfeasibility of recovering the xerogels from the treated stones, the xerogel obtained from the sol deposited on Petri dishes were characterized to gain information of the sample porosity, nano-structure and chemical reactivity. Firstly, the light absorption properties of the TiO_2-SiO_2 composited were studied. Our results, included in Figure S.5 and Table S.3, show that the band-gap of the raw titania nanosheets are not appreciably modified by the synthesis procedure of composite.

Figure S.6 shows the N_2 physisorption isotherms and the pore distribution, while Table 1 summarize the main textural data. All the isotherms correspond to Type IV (a), characteristic of mesoporous materials [29]. Type H1 hysteresis is shown by the samples containing P25, typically observed when the material is formed by the agglomeration of spherical nanoparticles [23]. The other samples exhibit Type H2 (b) hysteresis, that it is associated to the formation of ink bottle pores likely due to a partial pore blocking.

The pure silica xerogel exhibited a relatively high surface of 181 $m^2 \cdot g^{-1}$. The addition of P25 nanoparticles dramatically decrease the surface of the final composite to 41–36 $m^2 \cdot g^{-1}$. This effect is less intense when NS and NSNaOH are added and the surface are in all the cases higher than 100 $m^2 \cdot g^{-1}$. The samples containing P25 nanoparticles have longer gelation time, lower surface areas and bigger pore size (Figure S6) with respect to those of the nanosheets based system. This is an indication that the titania nanoparticles actively participate in the xerogel formation and determinate its final microstructure. According to our results, P25 negatively affect the growth of the SiO_2 xerogel and leads to slow formation rates and systems with bigger pores and lower surface area. This effect is more evident when the TiO_2 loading is increased and could be related with the adsorption of n-octylamine on the acidic site of TiO_2 P25. The addition of both as synthetized and washed nanosheets induced smaller changes in BET surface, while pore volume is significantly reduced (Figure S6). So, it can be considered that NS and NSNaOH catalyse the TES40 hydrolysis reducing the gelation time and generating more SiO_2 nucleation centres that leads to smaller particles and higher specific surface that in the case of the use of P25. A non-porous binder can dramatically reduce the photoactivity because it can inhibit the adsorption of the reactants on the active sites. Therefore, the porosity of the xerogels is a key factor for obtaining highly photoactive coating [37]. It has been previously reported that TiO_2-SiO_2 coatings, with a mesoporous structure similar to that of the present samples, exhibit better self-cleaning properties that the equivalent coatings with TiO_2 particles embedded in a microporous silica matrix [23]. O_2, water and NO are gas molecules with kinetic diameters below 0.35 nm and methylene blue has a 1.5x1 nm dimension. Therefore, the pore sizes of the present composites, which are higher than 8 nm, should allow a proper diffusion of the reactants onto the TiO_2 nanoparticles.

In order to gain information regarding the microstructure of the xerogels, the samples were intensively characterized by HAADF-STEM technique in combination with X-EDS analysis. This approach allows us to obtain composition maps of the different samples and determinate the distribution of the titania nanoparticles in the SiO_2 matrix. Fig. 4 includes representative HAADF images and the elemental mappings for Ti and Si for samples containing 4 wt% of TiO_2, the corresponding 1 wt% samples are compiled in Figure S.7. The HAADF-STEM images clearly show that the TiO_2 nanoparticles are integrated in a porous silica matrix. As it can be seen in Fig. 4 down, corresponding to sample S4NSNaOH, even some TNS are on the surface of the SiO_2 matrix. Images corresponding to samples S1NS and S4NS, especially the latter, demonstrate the agglomeration of titania nanosheets embedded in a porous silica matrix. This result is in good agreement with the dispersion problems that was observed during the synthesis of the gels containing as synthesised nanosheets. In contrast, the titania nanosheets are well dispersed after treating them with NaOH to remove the adsorbed fluorides, which increases the hydrophilicity of the materials.

3.3. Evaluation of the photo-induced elimination of colored organic molecules.

As previously described, the freshly prepared products were sprayed onto one of the biggest faces of 5x5x2 cm limestone blocks. The sol uptake for most of the samples were in the range of 29 to 33 mg/cm^2, the small differences observed are attributed to the heterogeneity inherent to the substrate. During the following days the weight of the samples decreased indicating that the xerogel formation was taking place. After two weeks, the weight remained constant at around 44–50 % of uptake values, which is near to the 41% of silica produced by the silica precursor. At that point the xerogel formation can be considered complete, associating the weight higher than the theoretical to ethanol occluded in the sample and non-hydrolyzed ethoxy groups that remains in the silica, and the changes in colour substrate induced by the treatments can be evaluated. All the ΔE* values measures for the samples were below 3 and thus, for similar substrates, there are no limitations for the application of these products related with changes of substrate appearance even in the most restrictive scenarios [38].

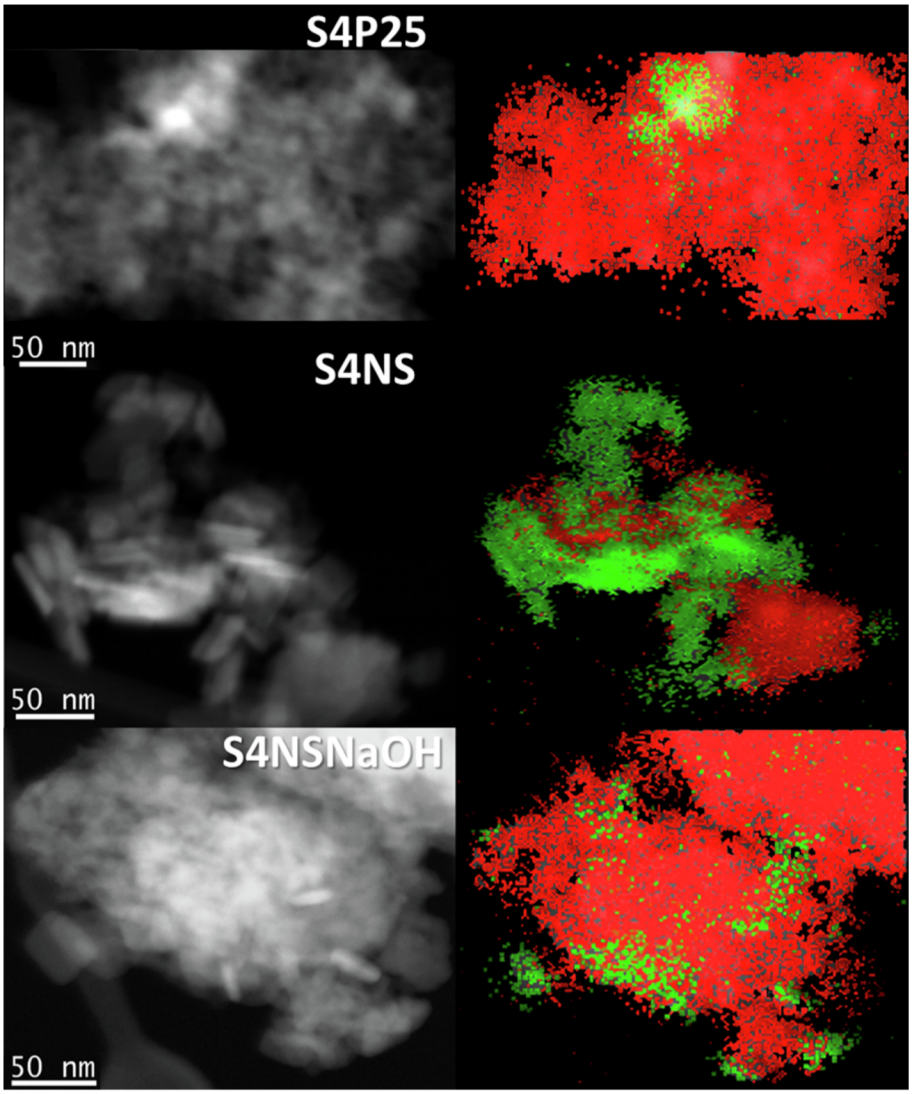

Fig. 4. Representative HAADF images (left) and elemental mapping (right) for Ti (green) and Si (red) of samples S4P25, S4NS and S4NSNaOH. (For interpretation of the references to color in this figure legend, the reader is referred to the web version of this article.)

In order to evaluate the photoactivity in the elimination of organic molecules of the coated samples, methylene blue photo-degradation tests were performed. Fig. 5 shows the photographs of the samples during the photocatalytic test. The included inset of each frame corresponds to a digital reproduction of the average colour of the surface of the stone from the colour coordinates measured by the colorimeter. We should point out that the MB is better dispersed on the untreated stones, since the treatments with xerogel prevent the penetration of MB solution in the substrate. As a result, MB is preferentially accumulated in some areas of the coating due to the sample surface heterogeneity. We observe how no visual changes were observed in the untreated sample during the experiment, while the surface of all the treated samples gradually get discoloured. On the other hand, if we compare the results obtained with pure SiO_2 coating (S) and TiO_2 containing coatings, it is also clear the positive effect of titania nanoparticles addition. It is noteworthy to mention the notable decolouration obtained in the case of the samples treated with S4NS and S4NSNaOH. In those cases, the stone recovered its initial colour in most part of the surface after 120 min. We also can conclude that the increase of the titania concentration favours the removal of MB.

In order to obtain quantitative results, a methodology based on taking the reflectance spectra of the samples during the photocatalytic decolourization was employed. This approach is based on the Kubelka-Munk theory, which was developed for modelling the optical properties of painted substrates [39,40]. According to this theory, the light absorption of a dye thin layer on a low absorbent substrate can be explained by the equation (1). Our system meets the requirements of this equation and therefore we can use it to obtain the equivalent MB absorption spectra that it can be used to determinate the concentration using the Lambert-Beer law. This methodology for quantifying the MB bleaching is better than others based on color coordinates changes [27].

$$F_{KM}(R) = \frac{(1-R)^2}{2R} \quad (1).$$

where $F_{KM}(R)$ is the Kubelka-Munk function (hereafter KM) that in our case is equivalent to absorbance and R is the absolute diffuse reflectance.

Figure 6.A includes the evolution of the UV–Vis spectra during the experiment carried out with sample S4NSNaOH. We can observe a main peak at ~665 nm and a shoulder at ~616 nm after the deposition of MB over the sample, i.e. time cero. According to the literature, the first peak can be related to the monomeric form of methylene blue and the latter to the dimeric form of the dye [41]. Similar spectra were obtained for all the SiO_2-TiO_2 composites (Figure S.8), although for the SiO_2 reference sample, the peak corresponding to the dimer is higher and remain similar during the reaction. In the case of the TiO_2 containing samples, the peak related to the monomer decreases faster than the one associated

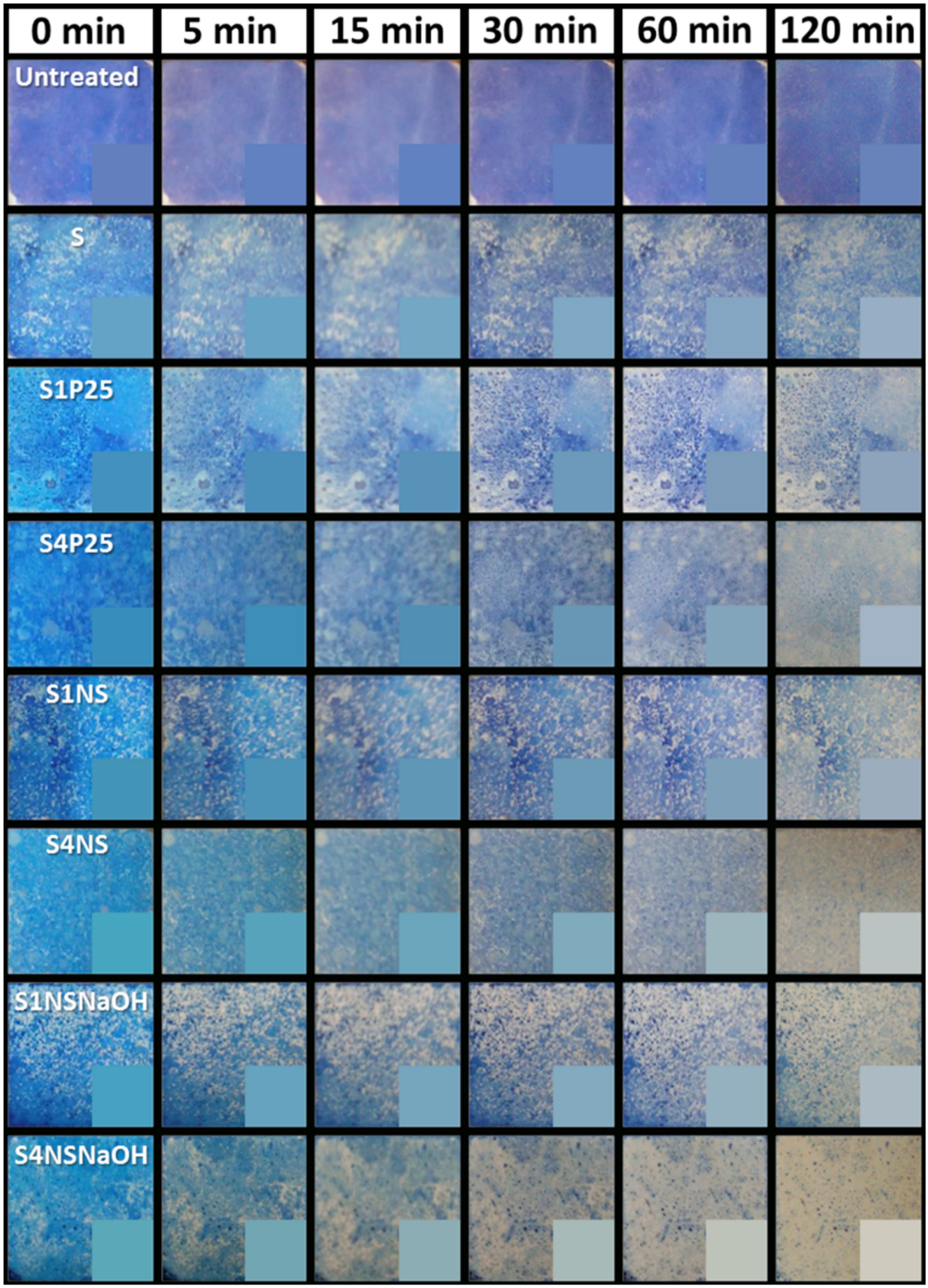

Fig. 5. Evolution of MB decolourization by photographs during the first 120 min of the photo-degradation test. The insets include the digital reproduction of the stone colour from the colour coordinates.

to the dimer, which indicates that its degradation is faster. However, the formation of intermediates such as azure A and azure B or even less cited in the literature azur C, thionine and phenothiazine cannot be excluded [42–44].

Figure 6.B includes the evolution of the absorbance (KM) normalized with respect to the initial absorbance (KM_0), both obtained at highest value of the absorption spectra. This curves allow us to determinate the decay of concentration of MB (the Kubelka-Munk equation employed also fits the Lambert-Beer equation) over time and we can easily compare the activity of the studied samples.

The low MB elimination on the untreated sample can be related with the spontaneous degradation of MB by simple UV light exposure due to purely photochemical mechanisms [45]. It is evident that the MB decolourization is greatly improved for the treated samples, even for S sample which is free of photoactive components. In this case, the MB degradation was also related to the photolysis, but the coating promoted the process because the MB remained in the external surface of material being more accessible to degradation and/or can be promoted by the acid sites on the surface of the SiO_2 coating, and, as it was previously discussed, MB is deposited in the coating as monomer, which is degraded faster than the dimer that is the predominant form in the untreated sample [27]. Despite this, it is clearly observed that the decolourization of MB is enhanced by adding TiO_2 nanoparticles, due to its photocatalytic properties. In fact, the performance of the coatings increases by increasing the amount of titania nanoparticles (Fig. 6.B).

If we consider the activity of the samples with the same amount of added titania nanoparticles, we can conclude that titania nanosheets exhibit better photocatalytic activity than the P25. On the other hand, the activity of the as synthetized nanosheets is improved by a pre-treatment with NaOH. The comparisons of the photocatalytic performance with the specific surface of the xerogels demonstrate that there is not any obvious correlation between them. We can observe, as example, that the sample S4P25 exhibits almost the same surface of the S1P25, but the catalytic performance of the first is better. A similar result is observed by adding as synthetized TiO_2 nanosheets and NaOH treated nanosheets the surface slightly changes (13%) by increasing the titania content, but the remaining MB is the double when we use the lower concentration. Therefore, we can conclude that the nature of the TiO_2 nanoparticles and the loading determinates the photocatalytic activity. P25 contains a mixture of anatase and rutile phases in a ratio of about 3 and an average particle sizes of 25 and 85 nm, respectively, while the NS and NSNaOH samples consists on pure anatase TiO_2 with exposed {0 0 1} and an average length of 35 nm and an average thickness of 6.5 nm. It has been previously reported that the coexistence of rutile and anatase has a beneficial on the catalytic tests [46]. On the other hand, recent research using morphologically controlled TiO_2 nanoparticles demonstrates that anatase {0 0 1} facets are highly active [24] in the oxidation of organic pollutants. The high density of surface undercoordinated Ti atoms on the {0 0 1} facets, compared to the {1 0 1} facets, improve the dissociative adsorption of reactants, such as formic acid, methanol and even water [47–50]. In addition, theoretical calculations indicates that the presence of large Ti–O–Ti bond angles promote the formation of very reactive 2p states linked to surface oxygen atoms [51]. Therefore, and despite the apparently contradictory published results, it is reasonable to expect that anatase nanoparticles with high percentage of {0 0 1} facets will exhibit high photocatalytic efficiency. Our results show that the nanosheets with a high content of {0 0 1} facets exhibit better catalytic performance than P25. If we compare the performance of P25 and the washed nanosheets, we can observe that the MB decolourization is greatly improved by using the washed nanosheets. In fact, after 30 min the stone treated with S4NSNaOH product show a value of KM/KM_0 almost thrice smaller that the value obtained for the stone treated with S4P25.

The effect of surface fluorination is also controversial. It is accepted that it affects the reactants adsorption, charge separation and transfer, and the reaction mechanism and kinetics. Recent studies demonstrate that depending on the oxidation mechanism, surface fluorination may either improve or inhibit the photocatalytic oxidation reactions [52,53]. Several works indicate that surface fluorination improves the photocatalytic degradation of organic compounds, such as phenol [54], benzoic acid [52] and some organic dyes [51,52] in water, when the reaction mechanism is based on the formation of •OH [53]. However, a negative effect has been observed when the reaction mechanism implies the absorption of the pollutants on the semiconductor in order to react

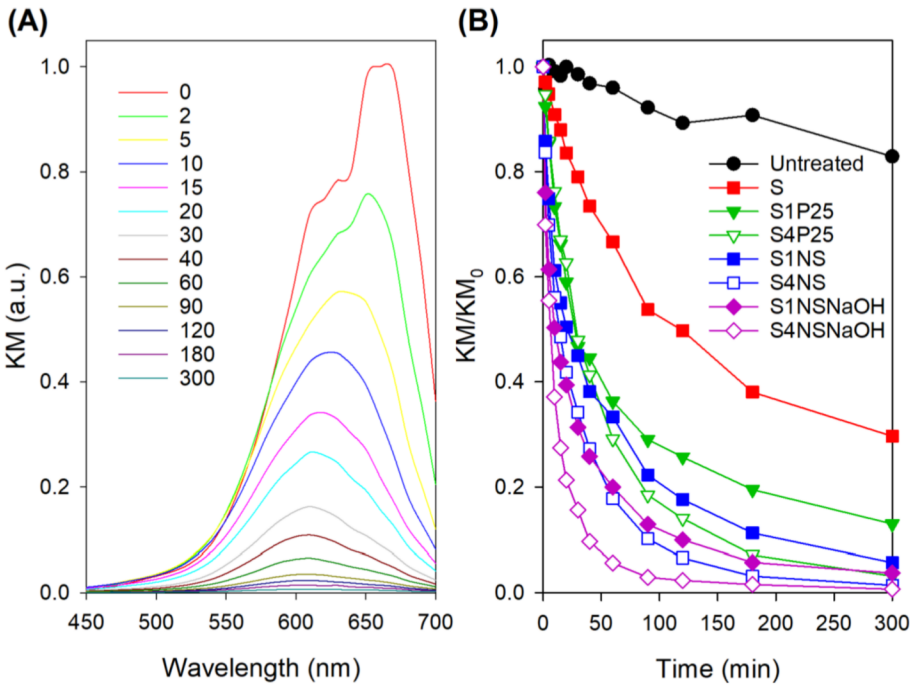

Fig. 6. UV–Vis spectra from Kubelka-Munk function obtained during the experiment carried out with sample S4NSNaOH (A) and KM/KM_0 at the maximum absorption over time for all the studied samples (B).

with the holes photoproduced in the semiconductor valence band. The explanation was related to the detrimental effects of the superficial fluorine to the reactants adsorption and the direct hole transfer to the organic substances [55]. Our results suggest that the reaction mechanism corresponds with the latter option and implies the direct adsorption on the catalyst surface. However, the worse distribution/dispersion of the un-washed titania nano-sheets within the xerogel and the deriving changes in textural properties may also be, at least partially, responsible of the lower activity exhibited by the samples containing the as-synthetized nanosheets in comparison with those obtained with washed nanosheets.

3.4. Photocatalytic elimination of soot.

The coating material with the best performance in decolourization of MB (S4NSNaOH) was selected to study the self-cleaning properties to remove soot, a real urban air pollutant that it is also a staining agent of buildings. An untreated limestone sample and one treated with S4P25 were employed as references materials. A thin layer of soot was deposited in order to slightly blacken the surface ensuring the light penetration until the treatment (see first column of Fig. 7.A). After 586 h of irradiation, no evident alteration of the soot stain on the untreated sample was observed with the naked eye but the stains on treated samples was lightened (see second column of Fig. 7.A). This stain elimination can be related to the oxidation of the soot to CO_2 [38].

The image treatment allowed to quantify the soot elimination as presented in Fig. 7.B. The color variation produced by the soot stain on the untreated sample was reduced by a 10% during the first 200 h, but after the color remained almost constant. This initial change of color can be related to an alteration of soot stain induced by the UV light rather than a real soot elimination. On the other hand, the color variation was considerably higher for the treated samples confirming the role of TiO_2 in the photocatalytic oxidation of soot. The S4P25 coating eliminated 30% of the soot whereas the coating containing the NSNaOH removed more than 50% of the stains. In this way, it is demonstrated that the highest photoactivity observed degrading MB also results in a higher elimination of organic molecules performance and therefore of self-cleaning performance.

3.5. Photocatalytic NO_x abatement.

The self-cleaning is not the only effect that a photocatalytic coating can provide to the building materials, the TiO_2 photoactivity is able to oxidize air pollutants producing building materials with depolluting properties. NO, a typical pollutant of urban and industrial areas, was chosen as model pollutant to assess the depolluting capabilities of building materials samples treated with S4NSNaOH product. The substrate employed was concrete because is the most abundant material in the NO_x emissions points and the application of a photocatalytic coating on its structures can help to mitigate the problems associated with high NO_x levels in the air. The obtained NO, NO_x and NO_2 concentration profiles for the samples treated with S4NSNaOH and S4P25, as reference material, are presented in Fig. 8.A, while the product distribution at the reaction outlet, NO conversion and NO_2 selectivity is plot in Fig. 8.B.

After the lamp was switched on, the NO content decreased fast and a minimum value of 580 ppb for S4P25 and 735 for S4NSNaOH were reached, which are translated in overall NO conversions of 36 and 24 % respectively. At the same time NO_2, an intermediate in the photooxidation process of NO to HNO_3 mediated by TiO_2 [56,57], started to be released but evident differences in the amount of this gas generated for each sample were observed. The final balance showed a total NO_x elimination of 22 and 21% for S4P25 and S4NSNaOH, respectively, and therefore both treatments have a similar capacity for removing NO_x. However, the selectivity of S4P25 to unwanted NO_2 is much higher than obtained for S4NSNaOH (39% vs 12%). For the S4P25 sample the concentration immediately reached the 60 ppb and it continued growing during the test up to 200 ppb, i.e. 14% of the initial NO concentration is transformed into NO_2. On the other hand, the NO_2 concentration for the S4NSNaOH sample was maintained under 60 ppb for all the duration of the test, which indicates that only 3% of the initial NO is converted into NO_2. In other words, both treatments have a similar NO_x depolluting performance, but S4NSNaOH released less NO_2 to the air. This is a key factor that must be consider to determine the potential real application of the photocatalyst because NO_2 (IDLH (immediately dangerous to life

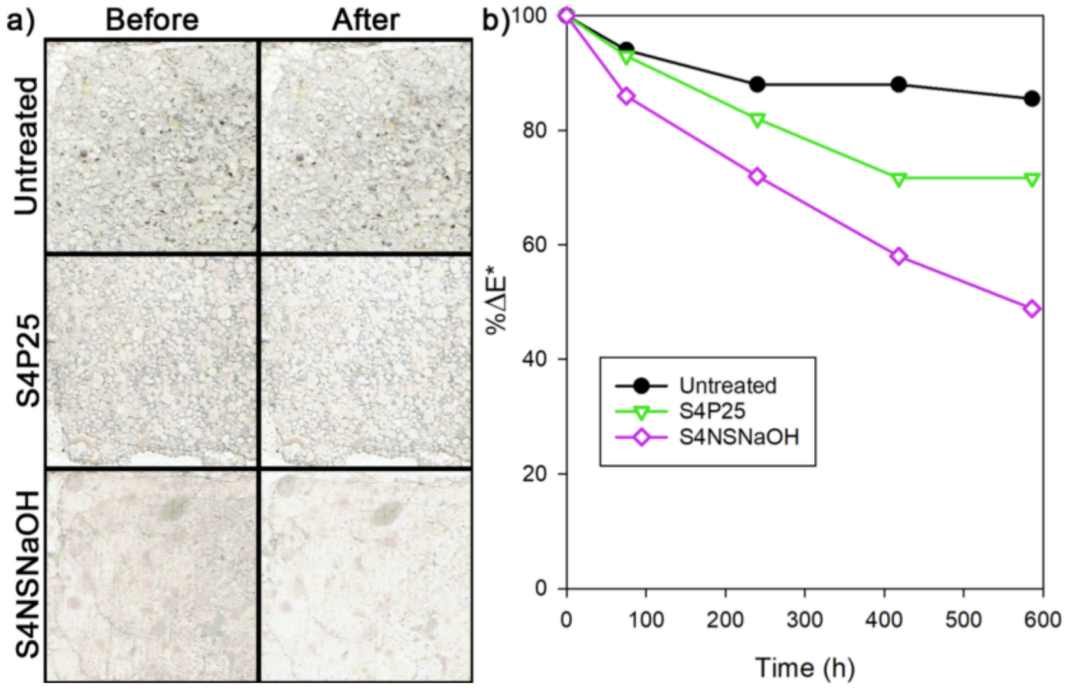

Fig. 7. Images showing the stone samples stained with soot before and after the UV irradiation (a) and evolution of ΔE% for the samples stained with soot during the UV irradiation (b).

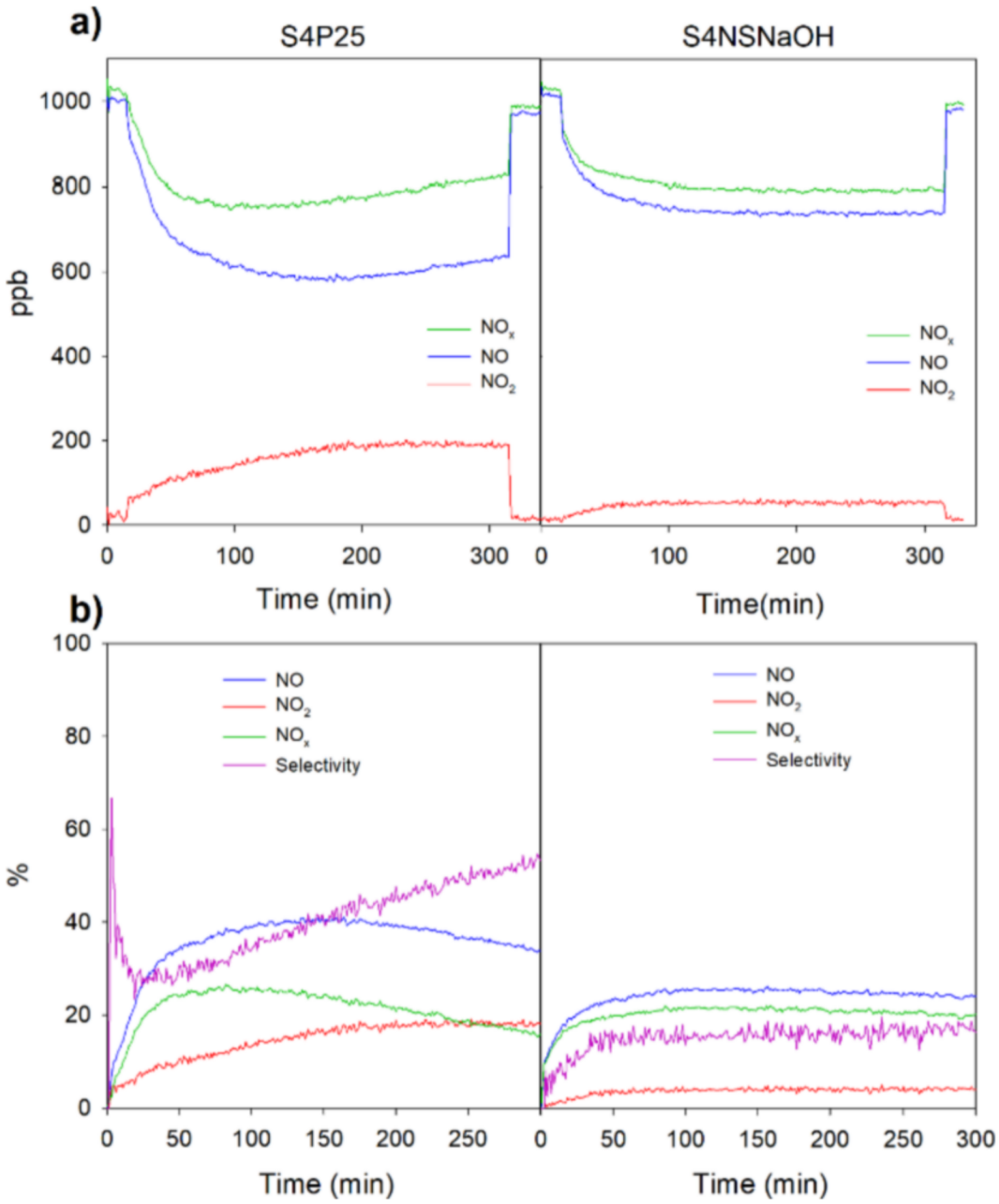

Fig. 8. Evolution of NO, NO_x and NO_2 concentrations during the NO photodegradation tests, the irradiation started at 15 min and switched off at 315 min (a). Progression of %NO conversion, $\%NO_2$ released, $\%NO_x$ removed and % selectivity to NO_2 during the irradiation of samples (b).

or health) value 20 ppm) has a toxicity 5 times higher than NO (IDLH value 100 ppm). For S4P25 sample the maximum efficiency of NO elimination is reached after approximately 90 min and later starts to slightly decrease. This decrease in the activity is even more obvious if we consider the NO_2 production. According to the green line in Fig. 8.B, this sample reach a maximum NO_x abatement of 26.5%, but later decreases to 15%. This result may be related with the photocatalyst deactivation due to the HNO_3 accumulation that promote the conversion of NO into NO_2 [58]. Regarding the S4NSNaOH, after 90 min the NOx elimination and NO_2 release remained almost unaffected, showing a remarkable photocatalytic stability. Photocatalytic paints prepared using P25 photocatalysts showed a NO_x abatement of 25% with a selectivity to NO_2 of 70–80% with a TiO_2 loading of 23 g/m^2 and a NO flow of 0.7 L/min [59]. By comparison, the coatings developed in this work with lower TiO_2 loading (16 g/m^2) and using a pollutant load much higher (8 μmol/h vs 1.9 μmol/h) achieved a similar NO_x abatement with less release of NO_2, demonstrating the benefits of employing a mesoporous silica matrix for producing photocatalytic coating over an organic binder. Therefore, it can be concluded that the synthetized nanosheets show promising results as component of photo-depolluting treatments for building materials.

4. Conclusions

Our results demonstrate that titania nanosheets can be used to obtain SiO_2-TiO_2 sols with the adequate viscosity, gelation time and photocatalytic properties to be used as an active element against air pollution, as well as self-cleaning protective material. Dispersing the as synthetized nanosheets particles was difficult due to the high content of fluorine on the surface of the sample that implies hydrophobic properties. This was corroborated by the characterization of the samples by EDS-STEM that showed the agglomeration of the TiO_2 nanosheets.

The obtained materials exhibit excellent photocatalytic properties, superior of that of the commercial P25 benckmark. The observed order in the dye removal activity of the synthetized products is the following:

S4NSNaOH > S4NS > S1NSNaOH > S4P25 > S1NSNaOH > S1P25 > S.

We demonstrated that the surface fluoration negatively affects the photocatalytic activity and that the activity of the titania nanosheets increases after washing with NaOH.

The samples prepared with titania nanosheets are also active in the photocatalytic abatement of NO_x, which it is a relevant reaction in air purification. More interestedly, concrete treated with titania nanosheets sols show a remarkable stability and a low NO_2 release, being both results of great interest for real applications.

The present work also clearly demonstrates that the use of morphologically controlled nanoparticles is a promising approach to develop novel products with improved photo-induced self-cleaning and depolluting activities. This approach is much appealing that others that introduce modifications in the band gap, such as doping, and provoke visible light absorption. It is obvious that the later approach leads to coloured materials that can modify the original colour of building materials. In the case of developing nanomaterial to protect heritage buildings, it is commonly accepted that the preservation of the original colour is mandatory.

Declaration of Competing Interest

The authors declare that they have no known competing financial interests or personal relationships that could have appeared to influence the work reported in this paper.

Acknowledgement

This work has been supported by the Ministry of Science and Innovation of Spain/FEDER Programm of the EU (ENE2017-82451-C3-2-R, PID2020-113809RB-C33 and PID2020-115843RB-I00/AEI/10.13039/501100011033) and the European Union under the 2014-2020 ERDF Operational Programme and by the Department of Economic Transformation, Industry, Knowledge, and Universities of the Regional Government of Andalusia (FEDER-UCA18-106613 and P18-RT-2727). J. J. Delgado thanks the "Ramón y Cajal" Program from MINECO/FEDER of Spain. M. Luna would also like to thank the Spanish Government for his Margarita Salas grant (2021-067/PN/MS-RECUAL/CD) supported by the European Union-NextGenerationEU. T.M. and P.F. acknowledge financial support from Ministry for University and Research (PRIN 2017PBXPN4).

References

[1] European Environment Agency (EEA), European Union emission inventory report 1990-2018 under the UNECE Convention on Long-range Transboundary Air Pollution (LRTAP), 2020. 10.2800/233574.

[2] L. Bauleo, S. Bucci, C. Antonucci, R. Sozzi, M. Davoli, F. Forastiere, C. Ancona, Long-term exposure to air pollutants from multiple sources and mortality in an industrial area: a cohort study, Occup. Environ. Med. 76 (2019) 48–57, https://doi.org/10.1136/oemed-2018-105059.

[3] European Environment Agency (EEA), Air quality in Europe - 2020 report, 2020. 10.2800/786656.

[4] F.M. Santos, Á. Gómez-Losada, J.C.M. Pires, Impact of the implementation of Lisbon low emission zone on air quality, J. Hazard. Mater. 365 (2019) 632–641, https://doi.org/10.1016/j.jhazmat.2018.11.061.

[5] S. Zhu, D. Wang, Photocatalysis: Basic Principles, Diverse Forms of Implementations and Emerging Scientific Opportunities, Adv. Energy Mater. 7 (2017) 1700841, https://doi.org/10.1002/aenm.201700841.

[6] M. Pelaez, N.T. Nolan, S.C. Pillai, M.K. Seery, P. Falaras, A.G. Kontos, P.S.M. M. Dunlop, J.W.J.J. Hamilton, J.A. Byrne, K. O'Shea, M.H. Entezari, D. D. Dionysiou, A review on the visible light active titanium dioxide photocatalysts for environmental applications, Appl. Catal. B Environ. 125 (2012) 331–349, https://doi.org/10.1016/j.apcatb.2012.05.036.

[7] J. Chen, C.S. Poon, Photocatalytic construction and building materials: From fundamentals to applications, Build. Environ. 44 (2009) 1899–1906, https://doi.org/10.1016/j.buildenv.2009.01.002.

[8] K. Januszkiewicz, P. Saricioglu, Towards Clean Air in Turkish Cities: Events in the Urban Space, IOP Conf. Ser. Mater. Sci. Eng. 603 (2019), 032101, https://doi.org/10.1088/1757-899X/603/3/032101.

[9] K. Januszkiewicz, K.G. Kowalski, Air Purification in Highly-Urbanized Areas with Use TiO2: New Approach to Design the Urban Public Space to Benefit Human Condition, IOP Conf. Ser. Mater. Sci. Eng. 603 (2019), 052071, https://doi.org/10.1088/1757-899X/603/5/052071.

[10] H. Park, Y. Park, W. Kim, W. Choi, Surface modification of TiO_2 photocatalyst for environmental applications, J. Photochem. Photobiol. C Photochem. Rev. 15 (2013) 1–20, https://doi.org/10.1016/j.jphotochemrev.2012.10.001.

[11] M. Luna, J.M. Gatica, H. Vidal, M.J. Mosquera, Use of Au/N-TiO2/SiO2 photocatalysts in building materials with NO depolluting activity, J. Clean. Prod. 243 (2020), 118633, https://doi.org/10.1016/j.jclepro.2019.118633.

[12] EN 15886: 2010; Conservation of cultural property - Test methods - Colour measurement of surfaces, (2010).

[13] C. Miliani, M.L. Velo-Simpson, G.W. Scherer, Particle-modified consolidants: A study on the effect of particles on sol-gel properties and consolidation effectiveness, J. Cult. Herit. 8 (2007) 1–6, https://doi.org/10.1016/j.culher.2006.10.002.

[14] K. Fischer, A. Gawel, D. Rosen, M. Krause, A. Abdul Latif, J. Griebel, A. Prager, A. Schulze, Low-temperature synthesis of anatase/rutile/brookite TiO_2 nanoparticles on a polymer membrane for photocatalysis, Catalysts. 7 (2017) 209, https://doi.org/10.3390/catal7070209.

[15] D.L. Liao, B.Q. Liao, Shape, size and photocatalytic activity control of TiO2 nanoparticles with surfactants, J. Photochem. Photobiol. A Chem. 187 (2007) 363–369, https://doi.org/10.1016/j.jphotochem.2006.11.003.

[16] T. Li, Z. Shen, Y. Shu, X. Li, C. Jiang, W. Chen, Facet-dependent evolution of surface defects in anatase TiO2 by thermal treatment: Implications for environmental applications of photocatalysis, Environ. Sci, Nano. 6 (2019) 1740–1753, https://doi.org/10.1039/c9en00264b.

[17] G. Liu, H.G. Yang, J. Pan, Y.Q. Yang, G.Q.M. Lu, H.-M. Cheng, Titanium Dioxide Crystals with Tailored Facets, Chem. Rev. 114 (2014) 9559–9612, https://doi.org/10.1021/cr400621z.

[18] L. Yang, F. Wang, C. Shu, P. Liu, W. Zhang, S. Hu, TiO<inf>2</inf>/porous cementitious composites: Influences of porosities and TiO<inf>2</inf> loading levels on photocatalytic degradation of gaseous benzene, Constr. Build. Mater. 150 (2017) 774–780, https://doi.org/10.1016/j.conbuildmat.2017.06.004.

[19] R. Paolini, D. Borroni, M. Pedeferri, M.V. Diamanti, Self-cleaning building materials: The multifaceted effects of titanium dioxide, Constr. Build. Mater. 182 (2018) 126–133, https://doi.org/10.1016/j.conbuildmat.2018.06.047.

[20] M.M. Hassan, H. Dylla, L.N. Mohammad, T. Rupnow, Evaluation of the durability of titanium dioxide photocatalyst coating for concrete pavement, Constr. Build. Mater. 24 (2010) 1456–1461, https://doi.org/10.1016/j.conbuildmat.2010.01.009.

[21] C. Mendoza, A. Valle, M. Castellote, A. Bahamonde, M. Faraldos, TiO_2 and TiO_2–SiO_2 coated cement: Comparison of mechanic and photocatalytic properties, Appl. Catal. B Environ. 178 (2015) 155–164, https://doi.org/10.1016/j.apcatb.2014.09.079.

[22] A. Calia, M. Lettieri, M. Masieri, Durability assessment of nanostructured TiO_2 coatings applied on limestones to enhance building surface with self-cleaning ability, Build. Environ. 110 (2016) 1–10, https://doi.org/10.1016/j.buildenv.2016.09.030.

[23] L. Pinho, M.J. Mosquera, Titania-silica nanocomposite photocatalysts with application in stone self-cleaning, J. Phys. Chem. C. 115 (2011) 22851–22862, https://doi.org/10.1021/jp2074623.

[24] H.G. Yang, C.H. Sun, S.Z. Qiao, J. Zou, G. Liu, S.C. Smith, H.M. Cheng, G.Q. Lu, Anatase TiO2 single crystals with a large percentage of reactive facets, Nature. 453 (2008) 638–641, https://doi.org/10.1038/nature06964.

[25] M. Luna, J.M. Gatica, H. Vidal, M.J. Mosquera, Au-TiO_2/SiO_2 photocatalysts with NO_x depolluting activity: Influence of gold particle size and loading, Chem. Eng. J. 368 (2019) 417–427, https://doi.org/10.1016/j.cej.2019.02.167.

[26] M. Thommes, B. Smarsly, M. Groenewolt, P.I. Ravikovitch, A.V. Neimark, Adsorption hysteresis of nitrogen and argon in pore networks and characterization of novel micro- and mesoporous silicas, Langmuir. 22 (2006) 756–764, https://doi.org/10.1021/la051686h.

[27] M. Luna, J. Delgado, M.L.A. Gil, M. Mosquera, TiO_2-SiO_2 coatings with a low content of AuNPs for producing self-cleaning building materials, Nanomaterials. 8 (2018) 177, https://doi.org/10.3390/nano8030177.

[28] ISO 22197-1: 2016; Fine ceramics (advanced ceramics, advanced technical ceramics) – Test method for air purification performance of semiconducting photocatalytic materials – Part 1: Removal of nitric oxide, 2016.

[29] M. Thommes, K. Kaneko, A.V. Neimark, J.P. Olivier, F. Rodriguez-Reinoso, J. Rouquerol, K.S.W. Sing, Physisorption of gases, with special reference to the evaluation of surface area and pore size distribution (IUPAC Technical Report), Pure Appl. Chem. 87 (2015) 1051–1069, https://doi.org/10.1515/pac-2014-1117.

[30] M. Fittipaldi, V. Gombac, A. Gasparotto, C. Deiana, G. Adami, D. Barreca, T. Montini, G. Martra, D. Gatteschi, P. Fornasiero, Synergistic Role of B and F Dopants in Promoting the Photocatalytic Activity of Rutile TiO2, ChemPhysChem. 12 (2011) 2221–2224, https://doi.org/10.1002/cphc.201100254.

[31] J. Tauc, R. Grigorovici, A. Vancu, Optical Properties and Electronic Structure of Amorphous Germanium, Phys. Status Solidi. 15 (1966) 627–637, https://doi.org/10.1002/pssb.19660150224.

[32] S.P. Tandon, J.P. Gupta, MEASUREMENT OF FORBIDDEN ENERGY GAP OF SEMICONDUCTORS BY DIFFUSE REFLECTANCE TECHNIQUE, Phys Status Solidi. 38 (1) (1970) 363–367.

[33] Q. Xiang, J. Yu, M. Jaroniec, Tunable photocatalytic selectivity of TiO2 films consisted of flower-like microspheres with exposed (001) facets, Chem. Commun. 47 (2011) 4532–4534, https://doi.org/10.1039/c1cc10501a.
[34] Y. Chen, F. Chen, J. Zhang, Effect of surface fluorination on the photocatalytic and photo-induced hydrophilic properties of porous TiO_2 films, Appl. Surf. Sci. 255 (12) (2009) 6290–6296, https://doi.org/10.1016/j.apsusc.2009.02.004.
[35] L. Pinho, F. Elhaddad, D.S. Facio, M.J. Mosquera, A novel TiO2–SiO2 nanocomposite converts a very friable stone into a self-cleaning building material, Appl. Surf. Sci. 275 (2013) 389–396, https://doi.org/10.1016/j.apsusc.2012.10.142.
[36] A. Prabhu, J.C. Gimel, A. Ayuela, J.S. Dolado, Effect of Nano Seeds in C-S-H Gel Formation: Simulation Study from the Colloidal Point of View, Concreep 10 (2015) 877–886, https://doi.org/10.1061/9780784479346.
[37] K. Nakamura, T. Yamaoka, T. Nagatsuka, Y. Taga, Binder Effect on Photocatalytic Performance of TiO 2, Solution Coating Layers 12 (2009) 15–18.
[38] A. Calia, M. Lettieri, M. Masieri, S Pal, A. Licciulli, V. Arima, J. Clean. Prod. 165 (2017) 1036–1047, https://doi.org/10.1016/j.jclepro.2017.07.193.
[39] P. Kubelka, F. Munk, Ein Beitrag zur Optik der Farbanstriche, Z. Tech. Phys. 12 (1931) 593–601.
[40] P. Kubelka, New Contributions to the Optics of Intensely Light-Scattering Materials. Part I, J. Opt. Soc. Am. 44 (1948) 448–457, https://doi.org/10.1364/JOSA.44.000330.
[41] G. Marbán, T.T. Vu, T. Valdés-Solís, A simple visible spectrum deconvolution technique to prevent the artefact induced by the hypsochromic shift from masking the concentration of methylene blue in photodegradation experiments, Appl. Catal. A Gen. 402 (2011) 218–223, https://doi.org/10.1016/j.apcata.2011.06.009.
[42] T. Zhang, T. Oyama, A. Aoshima, H. Hidaka, J. Zhao, N. Serpone, Photooxidative N-demethylation of methylene blue in aqueous TiO2 dispersions under UV irradiation, J. Photochem. Photobiol. A Chem. 140 (2001) 163–172, https://doi.org/10.1016/S1010-6030(01)00398-7.
[43] L. Yu, S. Yuan, L. Shi, Y. Zhao, J. Fang, Synthesis of Cu2+ doped mesoporous titania and investigation of its photocatalytic ability under visible light, Microporous Mesoporous Mater. 134 (2010) 108–114, https://doi.org/10.1016/j.micromeso.2010.05.015.
[44] Y. Tominaga, T. Kubo, K. Hosoya, Surface modification of TiO2 for selective photodegradation of toxic compounds, Catal. Commun. 12 (2011) 785–789, https://doi.org/10.1016/j.catcom.2011.01.021.
[45] A. Houas, Photocatalytic degradation pathway of methylene blue in water, Appl. Catal. B Environ. 31 (2001) 145–157, https://doi.org/10.1016/S0926-3373(00)00276-9.
[46] A. Beltram, I. Romero-Ocaña, J. Josè Delgado Jaen, T. Montini, P. Fornasiero, Photocatalytic valorization of ethanol and glycerol over TiO2 polymorphs for sustainable hydrogen production, Appl. Catal. A Gen. 518 (2016) 167–175.
[47] M. Lazzeri, A. Vittadini, A. Selloni, Structure and energetics of stoichiometric TiO2 anatase surfaces, Phys. Rev. B - Condens. Matter Mater. Phys. 63 (2001) 1554091–1554099, https://doi.org/10.1103/PhysRevB.63.155409.
[48] A. Vittadini, A. Selloni, F.P. Rotzinger, M. Grätzel, Structure and Energetics of Water Adsorbed at TiO2 Anatase (101) and (001) Surfaces, Phys. Rev. Lett. 81 (1998) 2954–2957, https://doi.org/10.1103/PhysRevLett.81.2954.
[49] X. Gong, A. Selloni, Reactivity of Anatase TiO Nanoparticles : The Role of the Minority (001) Surface Reactivity of Anatase TiO 2 Nanoparticles : The Role of the Minority (001) Surface, J. Phys. Chem. B. (2005) 1–4, https://doi.org/10.1021/jp055311g.
[50] C. Arrouvel, M. Digne, M. Breysse, H. Toulhoat, P. Raybaud, Effects of morphology on surface hydroxyl concentration: A DFT comparison of anatase-TiO2 and γ-alumina catalytic supports, J. Catal. 222 (2004) 152–166, https://doi.org/10.1016/j.jcat.2003.10.016.
[51] A. Tilocca, A. Selloni, Methanol adsorption and reactivity on clean and hydroxylated anatase(101) surfaces, J. Phys. Chem. B. 108 (2004) 19314–19319, https://doi.org/10.1021/jp046440k.
[52] M. Mrowetz, E. Selli, H2O2 evolution during the photocatalytic degradation of organic molecules on fluorinated TiO2, New J. Chem. 30 (2006) 108–114, https://doi.org/10.1039/B511320B.
[53] M. Mrowetz, E. Selli, Enhanced photocatalytic formation of hydroxyl radicals on fluorinated TiO2, Phys. Chem. Chem. Phys. 7 (2005) 1100–1102, https://doi.org/10.1039/b500194c.
[54] C. Minero, G. Mariella, V. Maurino, D. Vione, E. Pelizzetti, Photocatalytic transformation of organic compounds in the presence of inorganic ions. 2. Competitive reactions of phenol and alcohols on a titanium dioxide-fluoride system, Langmuir. 16 (2000) 8964–8972, https://doi.org/10.1021/la0005863.
[55] D. Monllor-Satoca, R. Gómez, M. González-Hidalgo, P. Salvador, The "Direct-Indirect" model: An alternative kinetic approach in heterogeneous photocatalysis based on the degree of interaction of dissolved pollutant species with the semiconductor surface, Catal. Today. 129 (2007) 247–255, https://doi.org/10.1016/j.cattod.2007.08.002.
[56] A. Mills, S. Elouali, The nitric oxide ISO photocatalytic reactor system: Measurement of NO_x removal activity and capacity, J. Photochem. Photobiol. A Chem. 305 (2015) 29–36, https://doi.org/10.1016/j.jphotochem.2015.03.002.
[57] S.Y. Kim, B.J. Cha, S. Zhao, H.O. Seo, Y.D. Kim, Photocatalytic activity of Fe-loaded TiO2 particles towards NO oxidation: Influence of the intrinsic structures, operating conditions, and synergic effects of the surface hardening agent, Constr. Build. Mater. 296 (2021), 123763, https://doi.org/10.1016/j.conbuildmat.2021.123763.
[58] Y. Ohko, Y. Nakamura, N. Negishi, S. Matsuzawa, K. Takeuchi, Photocatalytic oxidation of nitrogen monoxide using TiO_2 thin films under continuous UV light illumination, J. Photochem. Photobiol. A Chem. 205 (2009) 28–33, https://doi.org/10.1016/j.jphotochem.2009.04.005.
[59] C. Águia, J. Ângelo, L.M. Madeira, A. Mendes, Photo-oxidation of NO using an exterior paint - Screening of various commercial titania in powder pressed and paint films, J. Environ. Manage. (2011), https://doi.org/10.1016/j.jenvman.2011.02.010.